Projected West Antarctic ocean warming caused by an expansion of the Ross Gyre

Felipe Gomez-Valdivia[1], Paul Holland[1], Antony Siahaan[1], Pierre Dutrieux[1], and Emma F. Young[1]

[1]British Antarctic Survey

January 20, 2023

Abstract

We use the United Kingdom Earth System Model simulations from the Coupled Model Intercomparison Project 6 to analyse the dynamics of the Ross Gyre, West Antarctica, under historical and projected climate-change scenarios. During the historical period, the modelled Ross Gyre is relatively stable, with an extent and strength that are in reasonable agreement with observations. The projections exhibit an eastward gyre expansion into the Amundsen and Bellingshausen seas that starts during the 2040s. The associated cyclonic ocean circulation enhances the onshore transport of warm Circumpolar Deep Water into the eastern Amundsen Sea, a regime change that increases the subsurface shelf temperatures by up to 1.2*C and is independent of future forcing scenario. The Ross Gyre expansion is generated by a regional surface stress curl intensification associated with anthropogenic forcing. If realised in reality, such a warming would strongly influence the future stability of the West Antarctic Ice Sheet.

Projected West Antarctic ocean warming caused by an expansion of the Ross Gyre

Felipe Gómez-Valdivia[1], Paul R. Holland[1], Antony Siahaan[1], Pierre Dutrieux[1], Emma Young[1]

[1]British Antarctic Survey, Cambridge, UK

Key Points:

- The UK Earth System Model produces a realistic depiction of ocean and atmosphere conditions in West Antarctica.
- Future projections suggest a rapid warming of the Amundsen Sea induced by a Ross Gyre expansion that is independent of forcing scenario.
- The Ross Gyre expansion is caused by the surface stress curl intensification induced by anthropogenic trends in the westerly winds.

Corresponding author: Felipe Gómez-Valdivia, felmez@bas.ac.uk

Abstract

We use the United Kingdom Earth System Model simulations from the Coupled Model Intercomparison Project 6 to analyse the dynamics of the Ross Gyre, West Antarctica, under historical and projected climate-change scenarios. During the historical period, the modelled Ross Gyre is relatively stable, with an extent and strength that are in reasonable agreement with observations. The projections exhibit an eastward gyre expansion into the Amundsen and Bellingshausen seas that starts during the 2040s. The associated cyclonic ocean circulation enhances the onshore transport of warm Circumpolar Deep Water into the eastern Amundsen Sea, a regime change that increases the subsurface shelf temperatures by up to 1.2°C and is independent of future forcing scenario. The Ross Gyre expansion is generated by a regional surface stress curl intensification associated with anthropogenic forcing. If realised in reality, such a warming would strongly influence the future stability of the West Antarctic Ice Sheet.

Plain Language Summary

We use a climate model to analyse ocean changes around West Antarctica. Our results reveal a human-driven ocean warming that increases the continental shelf temperature in the Amundsen Sea by more than 1°C in only ∼30 years. This rapid warming is caused by a wind-driven expansion of the Ross Gyre, a large oceanic circulation in the region. The West Antarctic Ice Sheet is losing mass, causing sea-level rise, with the most rapid ice losses occurring in the Amundsen and Bellingshausen seas. Our results suggest that an expansion of the Ross Gyre could provide a mechanism whereby melt rates increase far beyond the current range. This could have an important influence on the sea-level rise caused by this region, with global impacts.

1 Introduction

The cyclonic Ross Gyre (RG) occupies the south-west Pacific sector of the Southern Ocean (Fig. 1a). Evidence from hydrographic data (Gouretski, 1999), satellite altimetry (Dotto et al., 2018), and modelling (Rickard et al., 2010) suggests the RG extends more than 3000 m below the ocean surface, with a transport of ∼20 Sv, dominating the large-scale thermohaline structure of the Ross Sea. The horizontal extent of the RG is limited by the continental shelf break to the south and west, and the Pacific–Antarctic Ridge to the north (Fig. 1a). The southward-flowing eastern limb is much less strongly constrained by topography (Patmore et al., 2019) and its location is more variable (Dotto et al., 2018; Sokolov & Rintoul, 2009). This eastern RG limb, and the adjacent Antarctic Circumpolar Current (ACC), supply warm Circumpolar Deep Water (CDW) to the Amundsen Sea shelf (Jenkins et al., 2016; Nakayama et al., 2018) that supports rapid melting when it reaches ice shelf cavities. Increases in such ocean-driven melting are known to be causing thinning of the ice sheet in the nearby Amundsen and Bellingshausen seas (Depoorter et al., 2013; Jenkins et al., 2016).

Satellite altimetry reveals variability in the RG strength and eastern boundary position (Dotto et al., 2018; Armitage et al., 2018; Sokolov & Rintoul, 2009) and numerical experiments have shown that the RG variability influences the water masses along the Amundsen Sea shelf (Nakayama et al., 2018). Any changes in the general circulation of this region may be of wide importance, considering the ocean-driven ice loss from West Antarctica during recent decades (Paolo et al., 2015) and the consequences for global sea-level rise (Shepherd et al., 2018).

In this study, we use numerical simulations of the United Kingdom Earth System Model (UKESM1) implementation for the Coupled Model Intercomparison Project 6 (CMIP6) (Sellar et al., 2020) to analyse the RG dynamics and its effects on the Amundsen and Bellingshausen seas. We consider historical simulations and two future climate scenarios associated with the Shared Socioeconomic Pathways SSP1-1.9 and SSP5-8.5 (Riahi et al., 2017). These SSPs are characterised by different fossil-fuel energy consumption leading to anthropogenic radiative forcing that diverges substantially after 2040 (O'Neill et al., 2016).

The following section includes a description of the UKESM1 simulations and the remote and in-situ observations that support our research. We first consider how well the model matches the observations. Next, we describe the historical and future evolution of the RG. Finally, we discuss the implications of these changes for ocean conditions and ice-sheet melting in the Amundsen Sea.

2 Methods

The UKESM1 is based on the HadGEM3-GC3.1 physical climate model (Kuhlbrodt et al., 2018) that simulates the coupled dynamics between land, atmosphere, ocean, and sea ice. Additionally, UKESM1 includes several Earth System components, including biogeochemical marine-terrestrial cycles, land-use management, and atmospheric chemistry (Sellar et al., 2020, 2019). The model variant UKESM1.1 includes an improved SO_2 parameterization (Hardacre et al., 2021) fundamental to produce a more realistic, up to $\sim$1°C warmer, surface averaged temperature in the extratropical Northern Hemisphere (UKESM, 2022); the averaged surface temperature differences between UKESM1 and UKESM1.1 within the Southern Hemisphere are, however, less than $\sim$0.1°C (UKESM, 2022); so for our purposes UKESM1 simulations are sufficient. A second model variant, UKESM1.0-ice, has been used to generate climate projections with an active Antarctic Ice Sheet model (Siahaan et al., 2021). UKESM1.0-ice simulations produce similar results to those described here, but we focus only on the UKESM1 because UKESM1.0-ice has not been used to produce historical simulations. The UKESM1 simulations analysed here necessarily have a relatively coarse resolution (1° ocean model), because higher-resolution UK climate models have substantial biases in the Southern Ocean (Andrews et al., 2020).

Under the SSP1-1.9 and the SSP5-8.5 scenarios, anthropogenic radiative forcing increases to $\sim$3.0 W m^{-2} by the 2030s (O'Neill et al., 2016); subsequently, due to strong emissions mitigation, the radiative forcing in SSP1-1.9 progressively decreases to only 1.9 W m^{-2} in 2100. By contrast, the SSP5-8.5 scenario is based on intensive fossil-fuel energy consumption and the anthropogenic radiative forcing continuously increases to 8.5 W m^{-2} in 2100 (O'Neill et al., 2016). We report ensembles of five 2015-2100 climate projections for each scenario, preceded by five historical 1850-2014 simulations.

We use a previously reported 2011-2016 Dynamic Ocean Topography (DOT) dataset from Cryosat-2 satellite data (Naveira Garabato et al., 2019) to evaluate the UKESM1 ocean surface geostrophic circulation. We subtracted 0.3 m from the modelled Sea Surface Height (SSH) to generate a modelled DOT for comparison. This correction is the mean difference between the satellite DOT and modelled SSH within the RG core, defined as the area delimited by the 15 Sv transport contour from the Barotropic Stream Function (BSF) (Fig. 1a). The 0 Sv transport contour (BSF_0) is used to identify the horizontal extent of the RG. DOT_2 indicates the -2 m DOT contour, previously associated with the surface signature of the southern ACC boundary (Naveira Garabato et al., 2019; Dotto et al., 2018; Armitage et al., 2018). We define the RG strength as being the maximum barotropic transport within the RG core. The poleward displacement of the Southern Hemisphere westerly jet is tracked using the maximum near-surface (10-m height) zonal wind velocity between 70°S and 45°S.

We use two different oceanographic datasets to evaluate the modelled regional thermohaline structure. For the deep ocean and RG, we use long-term 1955-2017 averages from the World Ocean Atlas 2018 (WOA) database (Garcia et al., 2019). For the Amundsen Sea shelf, we use long-term 1994-2018 averages of Austral-summer CTD observations (Dutrieux et al., 2014; Jenkins et al., 2018; Jacobs et al., 2011; Kim et al., 2021) interpolated onto a three-dimensional grid with a meridional and zonal resolutions of 0.06° and 0.2°, respectively, and a vertical resolution of 1 m. We compare the ETOPO1 seabed topography (Amante & Eakins, 2009) with the model bathymetry.

3 Validation of the UKESM1 dynamics

The modelled and satellite surface geostrophic circulation show a RG centered at ∼160°W and bordered by an ACC with geostrophic surface currents exceeding 10 cms^{-1} (Figs. 1a,d). The DOT_2 and BSF_0 contours are two measures of the horizontal RG extent, or equivalently the southern boundary of the Antartic Circumpolar Current (ACC). West of 145°W these contours follow the Pacific-Antarctic Ridge, illustrating how strongly the local bathymetry limits the extent of the RG (Figs. 1a,d). The eastern RG boundary is far less strongly constrained by bathymetry, with different measures from historical hydrographic data (Gouretski, 1999; Orsi et al., 1995; Chu & Fan, 2007) and altimetry (Dotto et al., 2018; Armitage et al., 2018) placing it at ∼140°W.

The modelled DOT_2 and BSF_0 exhibit a RG that, on average, extends to ∼140°W during 2011-2016 (Figs. 1d,e; magenta and green contours). The satellite DOT_2 and geostrophic circulation exhibit a surface RG expression extending to ∼135°W during the same period (Figs. 1a,b; red contour), suggesting that the modelled RG does not extend quite far enough eastward. This is confirmed by hydrographic evidence shown in the upper pannels of figure S1a: the WOA salinity distribution along section TS, at 135°W exhibits domed isohalines characteristic of the RG, while UKESM1 reproduces tilted isohalines along TS, characteristic of the ACC. The eastern boundary of the modelled RG during 2011-2016 is displaced westwards compared to observations, and this is important to our conclusions, as discussed below. However, the RG extent and strength in UKESM1 are still very realistic compared to many other climate models, which have extreme biases in this feature (Wang & Meredith, 2008).

Associated with the RG extension to ∼135°W (Fig. 1a), the altimetry circulation shows a bifurcation of the southward flow offshore of the shelf break, induced by the local bathymetry near TS at ∼69°S (Fig. 1b). The westward branch of this bifurcation follows the cyclonic RG circulation, while the eastward branch follows the ACC to the east around the Marie Byrd Seamounts (MBS) (Fig. 1b). The coarse UKESM1 bathymetry is smooth in this region (Fig. 1e), and the modelled surface ACC flow is unaffected by the seamounts. The modelled ACC flow reaches the shelf near 135°W, and dominates the upper shelf break surface circulation to the east (Fig. 1e). This is in agreement with altimetry observations in the Bellingshausen Sea, but not in the Amundsen Sea for this time period, as discussed below.

The UKESM1 produces a cyclonic gyre, hereafter referred to as the Amundsen Shelf Gyre (ASG), that appears in the barotropic stream function and dominates the surface geostrophic circulation over the Amundsen shelf around ∼110°W (Fig. 1e). Many regional models have highlighted a cyclonic barotropic circulation in this region, (e.g. Schodlok et al. (2012); Mathiot et al. (2017)), though the details of the circulation shown here reflect the coarse resolution and smooth shelf bathymetry in the UKESM1. Previous studies (e.g. Thoma et al. (2008); Dutrieux et al. (2014)) have concluded that ocean conditions on the Amundsen Sea shelf are influenced by zonal winds along the Amundsen shelf break. In turn, local zonal winds are characterised by energetic decadal variability around a mean of zero, and a centennial eastward trend of ∼0.4 m s^{-1} $century^{-1}$ driven by anthropogenic forcing (Holland et al., 2019). High resolution regional ocean simulations reproduce a historical Amundsen subsurface shelf warming trend of 0.33 °C $century^{-1}$ in response to eastward wind trends, of which approximately half is anthropogenically forced (Naughten et al., 2022). In agreement, the shelf break UKESM1 winds along the Amundsen Sea are also characterised by a historical eastward wind trend -not shown- and, as discussed below, UKESM1 produces an associated historical subsurface Amundsen shelf warming of ∼0.12°C $century^{-1}$.

The UKESM1 is known to have a good representation of water masses in the Pacific Sector of the Southern Ocean, which is not the case for many climate models (Heuzé, 2021; Purich & England, 2021). This is illustrated by the comparison of the observed and modelled thermohaline section along the transect T1 (Figs. 1c,f), located in the Dotson Trough (Fig. 1e). Model results exhibit warm CDW on the shelf, overlain by Winter Water and Antarctic Surface Water, as observed. In agreement with observations, the modelled CDW layer thickens towards the shelf (Figs. 1c,f). The properties of the modelled CDW are warmer and saltier and the modelled structure is smoother than observed (Figs. 1c,f), but overall the model performs remarkably well considering its coarse resolution and smooth bathymetry, visible when comparing the 3000 isobath in panels b and e of figure 1. As shown in the lower panels of figure S1b, along the transect T2 (Fig. 1e), the UKESM thermohaline distribution also agrees with observations along the Eastern Amundsen Sea shelf, the only other well-sampled section in the region.

The western shelf break circulation in the Amundsen Sea is characterized by a baroclinic current structure with a westward surface flow over an eastward undercurrent (Walker et al., 2013; A. F. Thompson et al., 2020) that is also reproduced by the UKESM1 (Figs. 2b), despite its coarse resolution.

4 Climatic changes within the UKESM1 simulations

In the historical simulations, the decadal-averaged BSF_0 implies a modelled RG that extends eastward to ∼130°W during the 1980s, before retreating to ∼140°W by the 2010s (Fig. 2a). Along the shelf-break, the westward barotropic flow within the RG weakens by the 2010s, while the eastward circulation outside the RG strengthens, with barotropic shelf currents exceeding 3 cms^{-1} along the Amundsen and Bellingshausen seas (Fig. 2a). On-shelf, the cyclonic ASG dominates the barotropic circulation throughout the 1980s-2010s period (Fig. 2a).

In the SSP1-1.9 projections, the BSF_0 contour reveals a connection between the RG and the ASG that initiates during the 2040s (Fig. 2a). The BSF_0 also suggests the development of a cyclonic gyre on the Bellingshausen Sea shelf during this period, hereafter referred to as the Bellingshausen Shelf Gyre (BSG), centered at ∼85°W (Fig. 2a).

By the 2070s, the interaction between the RG, the ASG, and the BSG, induces an overall cyclonic circulation that can be characterised as an eastward RG expansion into the Amundsen and Bellingshausen seas (Figs. 2a). The barotropic flows on-shelf are stronger and include a quasi-continuous westward inner-shelf current that reaches decadal averaged speeds larger than 2 cms^{-1} (Fig. 2a).

The evolution of zonal velocity along the transect T3, at the western Amundsen Sea shelf break, reflects the effects of these modelled RG changes. Before the 2000s, the local shelf break circulation is characterised by the westward Antarctic Slope Current flowing above an eastward undercurrent (Fig. 2b). This velocity shear is associated with the isopycnals sloping downwards to the south and, considering the coarseness of the model, is in remarkable agreement with previously reported observations (Walker et al., 2013; A. F. Thompson et al., 2020).

By the 2010s, the RG retreats westward to $\sim$140°W and a strengthened ACC over the shelf break induces a dominant barotropic eastward flow (Fig. 2a). The baroclinicity does not change substantially, so the maximum eastward flow is at depth (Fig. 2b) reaching up to 3 cms^{-1} at $\sim$500 m. After the 2040s, the RG expansion into the Amundsen Sea commences (Figs. 2a). The eastward barotropic flow first weakens, before dramatically changing from eastward to westward during the 2050s and 2060s (Fig. 2b). By the 2070s the local shelf break circulation becomes entirely westward, strongest at the surface due to the persistent baroclinic structure (Figs. 2b) associated with the effects of the cyclonic circulation on the subsurface isopycnals. There is a small projected increase in baroclinicity, but the dominant changes are barotropic.

The circulation of the Amundsen and Bellingshausen seas is driven by a cyclonic atmospheric circulation, the Amundsen Sea Low (Turner et al., 2013; Raphael et al., 2016), which comprises westerlies to the north and coastal easterlies to the south. Accordingly, the UKESM1 reproduces a regional Ocean Surface Stress Curl (OSC) that is preferentially cyclonic during the historical 1850-2014 period, with a local maximum near the shelf-break at $\sim$135°W (Fig. 3a).

The ocean surface stresses during the 1960s and the 2040s reveal a cyclonic intensification and a strengthening of the meridional stress gradient (Fig. 3a). Over the Amundsen-Bellinghausen domain shown in figure 3a, the OSC experiences an increasing cyclonicity that commences during the 1960s (Fig. 3b) and amplifies during the SSP scenarios to reach a regional average of $\sim 1.5\times10^{-7}$ N m^{-3} in the 2040s (Fig. 3b). Subsequently, the SSP1-1.9 cyclonic OSC progressively weakens to $\sim 1.3\times10^{-7}$ N m^{-3} by 2100, while the SSP5-8.5 cyclonic OSC strengthens further to reach an average $\sim 2\times10^{-7}$ N m^{-3} by 2100 (Fig. 3b). The OSC strengthening is primarily explained by stronger offshore westerlies (Fig. 3a) associated with the poleward displacement of the Southern Hemisphere westerly jet, a well-established atmospheric response to anthropogenic forcing (Bracegirdle et al., 2020; Holland et al., 2019; Goyal et al., 2021). As a result, the regional OSC strengthening follows the regional poleward displacement of the Southern Hemisphere westerly jet (Fig. S3).

A time series of the RG strength shows that it accelerates from a long-term average of ∼21 Sv during 1850-2000 to ∼32 Sv in SSP1-1.9 and ∼34 Sv in SSP5-8.5 (Fig. 3b) by 2100. During the historical 1851-1960 period the correlation between the OSC and the RG strength reaches up to ∼0.6 at the gyre core around 160°W (Fig. 3c), showing that the RG is driven by broad-scale winds over its entire extent. During 1961-2070 the intensification of the cyclonic OSC take place (Fig. 3b), and the correlation between the OSC and the RG strength reaches up to ∼0.9 along the Amundsen-Bellingshausen seas (Fig. 3d). This suggests that the regional near coastal cyclonic OSC intensification induces the RG strengthening and eastward extension onto the Amundsen-Bellinghausen seas, which occurs in both SSP scenarios (Fig. 2a).

As the RG intrusion starts to dominate the Amundsen and Bellingshausen seas in the projections, the inner-shelf temperature and salinity increases significantly, and this could have important implications for the West Antarctic Ice Sheet. Along transect T1, which crosses the cyclonic circulation induced by the RG intrusion into the Amundsen Sea (Figs. 1e,2a), the subsurface shelf warms by approximately 1°C between 1994-2018 and the 2070s (Figs. 1f, 4a), and the CDW layer thickness increases by approximately 200 m over the same period. The SSP5-8.5 experiment generates a more vigorous subsurface CDW penetration into the inner shelf and a stronger upper layer warming, due to a more energetic RG intrusion (Fig. 2) induced by an stronger OSC (Fig. 3b), but the difference between scenarios is small relative to the overall changes in both (Fig. 4b).

An enhanced inshore CDW penetration characterises the regional dynamics in both SSP scenarios. Between 135°W and 80°W and south of the 3000 m isobath the averaged subsurface potential temperature between 200 m and 700 m increases from a 1850-2014 average of ∼0.8°C to an average exceeding 2.0°C in the 2060s-2070s (Fig. 4b). Subsequently, the SSP1-1.9 temperatures decreased to ∼1.9°C by 2100; whereas, the SSP5-8.5 shelf temperatures continues increasing to ∼2.3°C by 2100. Comparison with the RG strength confirms that the energetic shelf warming along the Amundsen Sea shelf is induced by the enhancement and intrusion of the RG into the region (Fig. 4b). The long-term subsurface shelf warming trend during 1850-2014 period (Fig. 4b), shown by the green dashed line, is not explained by the RG strength, but by the previously reported (Holland et al., 2019; Naughten et al., 2022) long-term eastward trend of the zonal wind along the Amundsen Sea shelf break. Eastward wind trend also reproduced by the UKESM1 model.

5 Discussion

Previous studies describe decadal variability in the CDW transport into the Amundsen Sea, induced by atmospheric variability associated with the tropical Pacific (Thoma et al., 2008; Jenkins et al., 2016, 2018). In addition, Naughten et al. (2022) report a modelled wind-driven $\sim$0.33°C century^{-1} warming of the subsurface Amundsen Sea during 1920-2020. In agreement with these findings, the UKESM1 historical subsurface shelf temperature exhibits decadal variability superimposed upon a long-term $\sim$0.12°C century^{-1} warming (Fig. 4b). During the 2040s-2060s, a much more rapid shelf warming (Fig. 4b) is induced, however, by an eastward RG intrusion into the Amundsen and Bellingshausen seas (Fig. 2a). This represents an oceanic regime change that is completely outside the envelope of previously documented changes.

The eastward RG intrusion to the Amundsen and Bellingshausen seas is generated by the strengthening of the regional cyclonic Ocean Surface Stress Curl (OSC) (Figs. 3d). This OSC strengthening (Fig. 3b) is explained by the intensification of the regional westerlies (Fig. 3a) due to the poleward displacement of the Southern Hemisphere westerly jet, phenomena previously attributed to greenhouse gas increases and ozone depletion (D. W. J. Thompson et al., 2011; Bracegirdle et al., 2020; Goyal et al., 2021). As a result, the regional OSC derived from the SSP1-1.9 and SSP5-8.5 scenarios follow the associated anthropogenic radiative forcing shown in O'Neill et al. (2016, figure 3). However, we caution that, like several CMIP6 models, UKESM1 has a higher Equilibrium Climate Sensitivity compared to previous climate model generations (Sellar et al., 2019), which may be unrealistic (Forster et al., 2020). This means that the westerly wind changes over the Southern Ocean may well be over-estimated by these models.

The effects of reduced anthropogenic forcing in SSP1-1.9 are evident on the OSC after the 2060s, when the poleward westerly wind trends reverse (Fig. S3). As a result, the cyclonic OSC in SSP1-1.9 progressively becomes weaker (Fig. 3b) and the associated subsurface shelf temperature decrease by 30% during the following ∼40 years (Fig. 4b). However, these changes manifest too late to avoid the RG intrusion into the Amundsen-Bellingshausen seas (Fig. 2a) and the intensified shelf warming (Fig. 4).

During the 1980s the RG extended eastward of ∼130°W (Fig. 2a) and the eastern RG limb enhanced the westward Antarctic Slope Current along transect T3 (Fig. 2b). The dominance of the Antarctic Slope Current at T3 during 1850-2000 (Fig. 2b) suggests that this RG extent was prevalent during this period. Subsequently, however, the eastern RG boundary retreated westward to ∼140°W (Fig. 2a) and the ACC extended to the shelf break, strengthening the local undercurrent at T3 (Fig. 2b). This undercurrent intensification has been associated recently with the onshore CDW transport enhancement into the Amundsen shelf, which explains the increased ice shelf melting observed during recent decades (Naughten et al., 2022). Our results show that this undercurrent may be significantly affected by wider atmospheric and oceanic variability.

Satellite altimetry exhibits a bifurcation in the eastern RG limb at ∼69°S during 2011-2016, resulting in an ACC that travels north of the Marie Byrd Seamounts along the eastern side (Fig. 1b). This is not reproduced by the model during this time period, possibly due to the smooth model bathymetry and coarse resolution. The modelled shelf water mass distribution is broadly in agreement with the CTD observations (Figs. 1c,f), though the reproduced subsurface shelf water is, on average, warmer and saltier. Future research should focus on testing our findings within higher resolution models that better match the detailed oceanography and ice-shelf dynamics of this region.

6 Conclusions

We analyse the dynamics of the Ross Gyre (RG), West Antarctica, in the UK Earth System Model (UKESM1) under historical and climate change scenarios. We report, for the first time, a simulated expansion of the RG into the Amundsen and Bellingshausen seas, which is projected to occur around the 2040s in the model. This expansion is driven by a strengthening and poleward shift in the Southern Hemisphere westerly winds, a well-known climatic response to anthropogenic forcing.

This expansion of the RG enhances the onshore transport of warm Circumpolar Deep Water (CDW) into the Amundsen Sea, bringing much warmer CDW onto the shelf than is currently present. This increases the subsurface shelf temperature by more than

$\sim$1°C during the 2040-2070 period. This dramatic warming occurs irrespective of anthropogenic forcing scenario and, if realised, would have drastic consequences for melting of the West Antarctic Ice Sheet. These simulated future ocean changes are completely outside the envelope of both observed historical variability and previously modelled and inferred trends.

This coarse UKESM1 climate model performs remarkably well in many aspects of the oceanography of West Antarctica, though the modelled RG was slightly far west compared to observations, and the flow lacks sensitivity to local bathymetric features. For these reasons, we cannot be sure when or if the RG intrusion into the Amundsen and Bellingshausen seas is likely to take place. However, if such a phenomenon were to occur it would be fundamental to the future stability of the West Antarctic Ice Sheet. Further research into the feasibility of this oceanic regime change is urgently required.

7 Open Research

Historical UKESM1 data can be accessed at MOHC (2019a); whereas, MOHC (2019c) and MOHC (2019b) offer access to SSP1-1.9 and SSP5-8.5 UKESM1 projections, respectively.

Acknowledgments

The UKESM development group reproduced the UKESM1 data reported here. We accessed WOA data through the website https://www.ncei.noaa.gov/access/world-ocean-atlas-2018/. Tiago Dotto kindly provided monthly averaged 2011-2016 Cryosat-2 satellite data. Most data analysis and figures were generated using the NOAA-PMEL Ferret application under the UK's high performance computing JASMIN facility. We thank Robin Smith for his helpful comments and suggestions about our research.

References

Amante, C., & Eakins, B. (2009). *ETOPO1 1 Arc-Minute Global Relief Model: Procedures, data sources and analysis* (Tech. Rep.). NOAA National Geophysical Data Center. doi: doi:10.7289/V5C8276M

Andrews, M. B., Ridley, J. K., Wood, R. A., Andrews, T., Blockley, E. W., Booth, B., ... Sutton, R. T. (2020). Historical Simulations With HadGEM3-GC3.1 for CMIP6. *Journal of Advances in Modeling Earth Systems*, *12*(6), e2019MS001995. doi: https://doi.org/10.1029/2019MS001995

Armitage, T. W. K., Kwok, R., Thompson, A. F., & Cunningham, G. (2018). Dynamic Topography and Sea Level Anomalies of the Southern Ocean: Variability and Teleconnections. *Journal of Geophysical Research: Oceans*, *123*(1), 613-630. doi: https://doi.org/10.1002/2017JC013534

Bracegirdle, T. J., Krinner, G., Tonelli, M., Haumann, F. A., Naughten, K. A., Rackow, T., ... Wainer, I. (2020). Twenty first century changes in Antarctic and Southern Ocean surface climate in CMIP6. *Atmospheric Science Letters*, *21*(9), e984. doi: https://doi.org/10.1002/asl.984

Chu, P. C., & Fan, C. (2007). An inverse model for calculation of global volume transport from wind and hydrographic data. *Journal of Marine Systems*, *65*(1), 376-399. doi: https://doi.org/10.1016/j.jmarsys.2005.06.010

Depoorter, M. A., Bamber, J. L., Griggs, J. A., Lenaerts, J. T. M., Ligtenberg, S. R. M., & van den Broeke, M. R. (2013). Calving fluxes and basal melt rates of Antarctic ice shelves. *Nature*, *502*, 89-92. doi: 10.1038/nature12567

Dotto, T. S., Naveira Garabato, A., Bacon, S., Tsamados, M., Holland, P. R., Hooley, J., ... Meredith, M. P. (2018). Variability of the Ross Gyre, Southern Ocean: Drivers and Responses Revealed by Satellite Altimetry. *Geophysical Research Letters*, *45*(12), 6195-6204. doi: https://doi.org/10.1029/2018GL078607

Dutrieux, P., Rydt, J. D., Jenkins, A., Holland, P. R., Ha, H. K., Lee, S. H., ... Schröder, M. (2014). Strong sensitivity of Pine Island ice-shelf melting to climatic variability. *Science*, *343*(6167), 174-178. doi: 10.1126/science.1244341

Forster, P. M., Maycock, A. C., McKenna, C. M., & Smith, C. J. (2020). Latest climate models confirm need for urgent mitigation. *Nature Climate Change*, *10*, 7-10. doi: 10.1038/s41558-019-0660-0

Garcia, H., Boyer, T. P., Locarnini, R. A., Mishonov, A., Grodsky, C., Weathers, K. A., ... Zweng, M. M. (2019). *World Ocean Atlas 2018: product documentation* (Tech. Rep.). Boulder, Colorado: NOAA National Centers for Environmental Information.

Gouretski, V. (1999). The large-scale thermohaline structure of the Ross Gyre. In G. Manzella (Ed.), *Oceanography of the ross sea antarctica.* Milano: Springer. doi: https://doi.org/10.1007/978-88-470-2250-8_6

Goyal, R., Sen Gupta, A., Jucker, M., & England, M. H. (2021). Historical and projected changes in the Southern Hemisphere surface westerlies. *Geophysical Research Letters*, *48*(4), e2020GL090849. doi: https://doi.org/10.1029/2020GL090849

Hardacre, C., Mulcahy, J. P., Pope, R. J., Jones, C. G., Rumbold, S. T., Li, C., … Turnock, S. T. (2021). Evaluation of so_2, so_4^{2-} and an updated so_2 dry deposition parameterization in the united kingdom earth system model. *Atmospheric Chemistry and Physics*, *21*(24), 18465–18497. Retrieved from `https://acp.copernicus.org/articles/21/18465/2021/` doi: 10.5194/acp-21-18465-2021

Heuzé, C. (2021). Antarctic Bottom Water and North Atlantic Deep Water in CMIP6 models. *Ocean Science*, *17*(1), 59–90. Retrieved from `https://os.copernicus.org/articles/17/59/2021/` doi: 10.5194/os-17-59-2021

Holland, P. R., Bracegirdle, T. J., Dutrieux, P., Jenkins, A., & Steig, E. J. (2019). West Antarctic ice loss influenced by internal climate variability and anthropogenic forcing. *Nature Geoscience*, *12*, 718-724. doi: {10.1038/s41561-019-0420-9}

Jacobs, S. S., Jenkins, A., Giulivi, C. F., & Dutrieux, P. (2011). Stronger ocean circulation and increased melting under Pine Island Glacier ice shelf. *Nature Geoscience*, *4*, 519-523. doi: 10.1038/ngeo1188

Jenkins, A., Dutrieux, P., Jacobs, S., Steig, E. J., Gudmundsson, G. H., Smith, J., & Heywood, K. J. (2016, December). Decadal Ocean Forcing and Antarctic Ice Sheet Response: Lessons from the Amundsen Sea. *Oceanography*. doi: https://doi.org/10.5670/oceanog.2016.103

Jenkins, A., Shoosmith, D., Dutrieux, P., Jacobs, S., Kim, T. W., Lee, S. H., … Stammerjohn, S. (2018). West Antarctic Ice Sheet retreat in the Amundsen Sea driven by decadal oceanic variability. *Nature Geoscience*, *11*(1752-0908), 733-738. doi: 10.1038/s41561-018-0207-4

Kim, T.-W., Yang, H. W., Dutrieux, P., Wåhlin, A. K., Jenkins, A., Kim, Y. G., … Cho, Y.-K. (2021). Interannual Variation of Modified Circumpolar Deep Water in the Dotson-Getz Trough, West Antarctica. *Journal of Geophysical Research: Oceans*, *126*(12), e2021JC017491. doi: https://doi.org/10.1029/2021JC017491

Kuhlbrodt, T., Jones, C. G., Sellar, A., Storkey, D., Blockley, E., Stringer, M., … Walton, J. (2018). The Low-Resolution Version of HadGEM3 GC3.1: Development and Evaluation for Global Climate. *Journal of Advances in Modeling Earth Systems*, *10*(11), 2865-2888. Retrieved from `https://agupubs.onlinelibrary.wiley.com/doi/abs/10.1029/2018MS001370` doi: https://doi.org/10.1029/2018MS001370

Mathiot, P., Jenkins, A., Harris, C., & Madec, G. (2017). Explicit representation and parametrised impacts of under ice shelf seas in the z^* coordinate ocean model NEMO 3.6. *Geoscientific Model Development*, *10*(7), 2849–2874. Retrieved from `https://gmd.copernicus.org/articles/10/2849/2017/` doi: 10.5194/gmd-10-2849-2017

MOHC. (2019a). *Met Office Hadley Centre (MOHC) UKESM1-0-LL model output for the "historical" experiment* [dataset]. Retrieved from `https://catalogue.ceda.ac.uk/uuid/59c10ac7bea2424f8eb64f0e310a2d4f` (May 2021)

MOHC. (2019b). *Met Office Hadley Centre (MOHC) UKESM1-0-LL model output for the "historical" experiment* [dataset]. Retrieved from `http://catalogue.ceda.ac.uk/uuid/dd5bd2e874a44a0db9b0757d633c212c` (May 2021)

MOHC. (2019c). *WCRP CMIP6: Met Office Hadley Centre (MOHC) UKESM1-0-LL model output for the "ssp119" experiment.* [dataset]. Retrieved from `https://catalogue.ceda.ac.uk/uuid/7910bf8499c34c87a0bd4402402465a2` (May 2021)

Nakayama, Y., Menemenlis, D., Zhang, H., Schodlok, M., & Rignot, E. (2018). Origin of Circumpolar Deep Water intruding onto the Amundsen and Bellingshausen Sea continental shelves. *Nature Communications*, *9*, 3403. doi: https://doi.org/10.1038/s41467-018-05813-1

Naughten, K. A., Holland, P. R., Dutrieux, P., Kimura, S., Bett, D. T., & Jenkins, A. (2022). Simulated Twentieth-Century Ocean Warming in the Amundsen Sea, West Antarctica. *Geophysical Research Letters*, *49*(5), e2021GL094566. doi: https://doi.org/10.1029/2021GL094566

Naveira Garabato, A. C., Dotto, T. S., Hooley, J., Bacon, S., Tsamados, M., Ridout, A., … Meredith, M. P. (2019). Phased Response of the Subpolar Southern Ocean to Changes in Circumpolar Winds. *Geophysical Research Letters*, *46*(11), 6024-6033. doi: https://doi.org/10.1029/2019GL082850

O'Neill, B. C., Tebaldi, C., van Vuuren, D. P., Eyring, V., Friedlingstein, P., Hurtt, G., ... Sanderson, B. M. (2016). The Scenario Model Intercomparison Project (ScenarioMIP) for CMIP6. *Geoscientific Model Development*, *9*(9), 3461–3482. Retrieved from `https://gmd.copernicus.org/articles/9/3461/2016/` doi: 10.5194/gmd-9-3461-2016

Orsi, A. H., Whitworth, T., & Nowlin, W. D. (1995). On the meridional extent and fronts of the Antarctic Circumpolar Current. *Deep Sea Research Part I: Oceanographic Research Papers*, *42*(5), 641-673. Retrieved from `https://www.sciencedirect.com/science/article/pii/096706379500021W` doi: https://doi.org/10.1016/0967-0637(95)00021-W

Paolo, F. S., Fricker, H. A., & Padman, L. (2015). Volume loss from Antarctic ice shelves is accelerating. *Science*, *348*(6232), 327-331. doi: 10.1126/science.aaa0940

Patmore, R. D., Holland, P. R., Munday, D. R., Naveira Garabato, A. C., Stevens, D. P., & Meredith, M. P. (2019). Topographic Control of Southern Ocean Gyres and the Antarctic Circumpolar Current: A Barotropic Perspective. *J. Phys. Ocean.*, *49*(12), 3221–3244. doi: 10.1175/JPO-D-19-0083.1

Purich, A., & England, M. H. (2021). Historical and future projected warming of Antarctic Shelf Bottom Water in CMIP6 models. *Geophysical Research Letters*, *48*(10), e2021GL092752. doi: https://doi.org/10.1029/2021GL092752

Raphael, M. N., Marshall, G. J., Turner, J., Fogt, R. L., Schneider, D., Dixon, D. A., ... Hobbs, W. R. (2016). The Amundsen Sea Low: Variability, Change, and Impact on Antarctic Climate. *Bulletin of the American Meteorological Society*, *97*(1), 111 - 121. doi: 10.1175/BAMS-D-14-00018.1

Riahi, K., van Vuuren, D. P., Kriegler, E., Edmonds, J., O'Neill, B. C., Fujimori, S., ... Tavoni, M. (2017). The Shared Socioeconomic Pathways and their energy, land use, and greenhouse gas emissions implications: An overview. *Global Environmental Change*, *42*, 153-168. Retrieved from `https://www.sciencedirect.com/science/article/pii/S0959378016300681` doi: https://doi.org/10.1016/j.gloenvcha.2016.05.009

Rickard, G. J., Roberts, M. J., Williams, M. J., Dunn, A., & Smith, M. H. (2010). Mean circulation and hydrography in the Ross Sea sector, Southern Ocean: representation in numerical models. *Antarctic Science*, *22*(5), 533–558. doi:

10.1017/S0954102010000246

Schodlok, M. P., Menemenlis, D., Rignot, E., & Studinger, M. (2012). Sensitivity of the ice-shelf/ocean system to the sub-ice-shelf cavity shape measured by NASA IceBridge in Pine Island Glacier, West Antarctica. *Annals of Glaciology*, *53*(60), 156–162. doi: 10.3189/2012AoG60A073

Sellar, A. A., Jones, C. G., Mulcahy, J. P., Tang, Y., Yool, A., Wiltshire, A., … Zerroukat, M. (2019). UKESM1: Description and Evaluation of the U.K. Earth System Model. *Journal of Advances in Modeling Earth Systems*, *11*(12), 4513-4558. Retrieved from `https://agupubs.onlinelibrary.wiley.com/doi/abs/10.1029/2019MS001739` doi: https://doi.org/10.1029/2019MS001739

Sellar, A. A., Walton, J., Jones, C. G., Wood, R., Abraham, N. L., Andrejczuk, M., … Griffiths, P. T. (2020). Implementation of U.K. Earth System Models for CMIP6. *Journal of Advances in Modeling Earth Systems*, *12*(4), e2019MS001946. Retrieved from `https://agupubs.onlinelibrary.wiley.com/doi/abs/10.1029/2019MS001946` (e2019MS001946 10.1029/2019MS001946) doi: https://doi.org/10.1029/2019MS001946

Shepherd, A., Ivins, E., Rignot, E., Smith, B., van den Broeke, M., Velicogna, I., & Et, a. (2018). Mass balance of the Antarctic Ice Sheet from 1992 to 2017. *Nature*, *558*(6232), 219-222. doi: 10.1038/s41586-018-0179-y

Siahaan, A., Smith, R., Holland, P., Jenkins, A., Gregory, J. M., Lee, V., … Jones, C. (2021). The Antarctic contribution to 21st century sea-level rise predicted by the UK Earth System Model with an interactive ice sheet. *The Cryosphere Discussions*, *2021*, 1–42. Retrieved from `https://tc.copernicus.org/preprints/tc-2021-371/` doi: 10.5194/tc-2021-371

Sokolov, S., & Rintoul, S. R. (2009). Circumpolar structure and distribution of the Antarctic Circumpolar Current fronts: 2. Variability and relationship to sea surface height. *Journal of Geophysical Research: Oceans*, *114*(C11). doi: https://doi.org/10.1029/2008JC005248

Thoma, M., Jenkins, A., Holland, D., & Jacobs, S. (2008). Modelling Circumpolar Deep Water intrusions on the Amundsen Sea continental shelf, Antarctica. *Geophysical Research Letters*, *35*(18). doi: https://doi.org/10.1029/2008GL034939

Thompson, A. F., Speer, K. G., & Schulze Chretien, L. M. (2020). Genesis of the Antarctic Slope Current in West Antarctica. *Geophysical Research Letters*, *47*(16), e2020GL087802. doi: https://doi.org/10.1029/2020GL087802

Thompson, D. W. J., Solomon, S., Kushner, P. J., England, M. H., Grise, K. M., & Karoly, D. J. (2011). Signatures of the Antarctic ozone hole in Southern Hemisphere surface climate change. *Nature Geoscience*, *4*, 741-749. doi: 10.1038/ngeo1296

Turner, J., Phillips, T., Hosking, J. S., Marshall, G. J., & Orr, A. (2013). The Amundsen Sea low. *International Journal of Climatology*, *33*(7), 1818-1829. doi: https://doi.org/10.1002/joc.3558

UKESM. (2022, Dec. 22,). *United Kingdom Earth System Modelling (UKESM).* Retrieved from `https://ukesm.ac.uk/portfolio-item/introducing-ukesm1-1-a-new-configuration-of-the-ukesm-model-with-an-improved-historical-temperature-record/`

Walker, D. P., Jenkins, A., Assmann, K. M., Shoosmith, D. R., & Brandon, M. A. (2013). Oceanographic observations at the shelf break of the Amundsen Sea, Antarctica. *Journal of Geophysical Research: Oceans*, *118*(6), 2906-2918. doi: https://doi.org/10.1002/jgrc.20212

Wang, Z., & Meredith, M. P. (2008). Density-driven Southern Hemisphere subpolar gyres in coupled climate models. *Geophysical Research Letters*, *35*(14). doi: https://doi.org/10.1029/2008GL034344

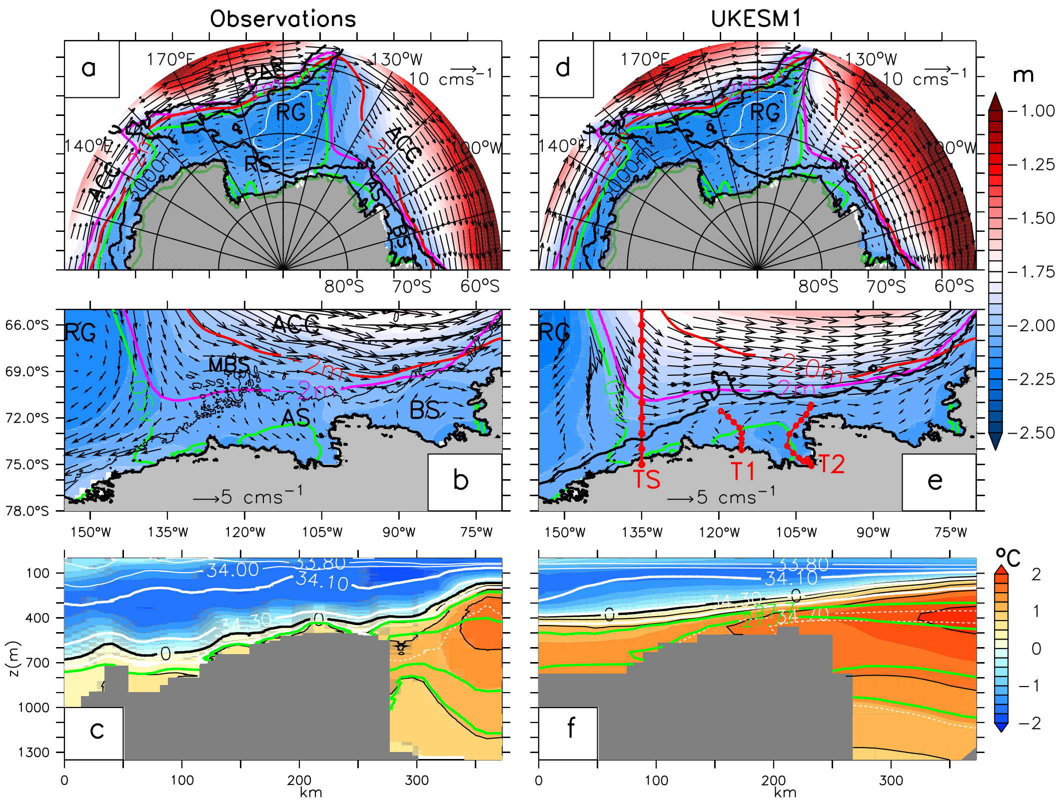

Figure 1. (a) Mean satellite DOT [m] and derived surface geostrophic currents [cms^{-1}] in the South Pacific. The mean satellite DOT_2 is in red and the ensemble-means of modelled BSF_0 and DOT_2 are shown in green and magenta, respectively. The 3000 m isobath from ETOPO1 is in black, and the white line delimits the mean modelled RG core. (b) Same as panel a, but for the Amundsen-Bellingshausen seas region. The locations of the Ross Gyre (RG), Ross Sea (RS), Pacific-Antarctic Ridge (PAR), Amundsen Sea (AS), Bellingshausen Sea (BS), Marie Byrd Seamounts (MBS), and the ACC are shown in panels a and b. (c) The averaged austral-summer thermohaline structure in the upper 1300 m along transect T1 from CTD data. Potential temperature [°C] is shown in color and black contours, white contours exhibit isohalines [psu], green countours show the 27.7, 27.77, 27.81, and 27.82 potential density anomaly isopycnals [kg m^{-3}]. (d), (e), and (f) are equivalent to (a), (b) and (c), respectively, but for the modelled ensemble means and the model's 3000 m isobath. Transects TS, T1, and T2 are shown in panel e.

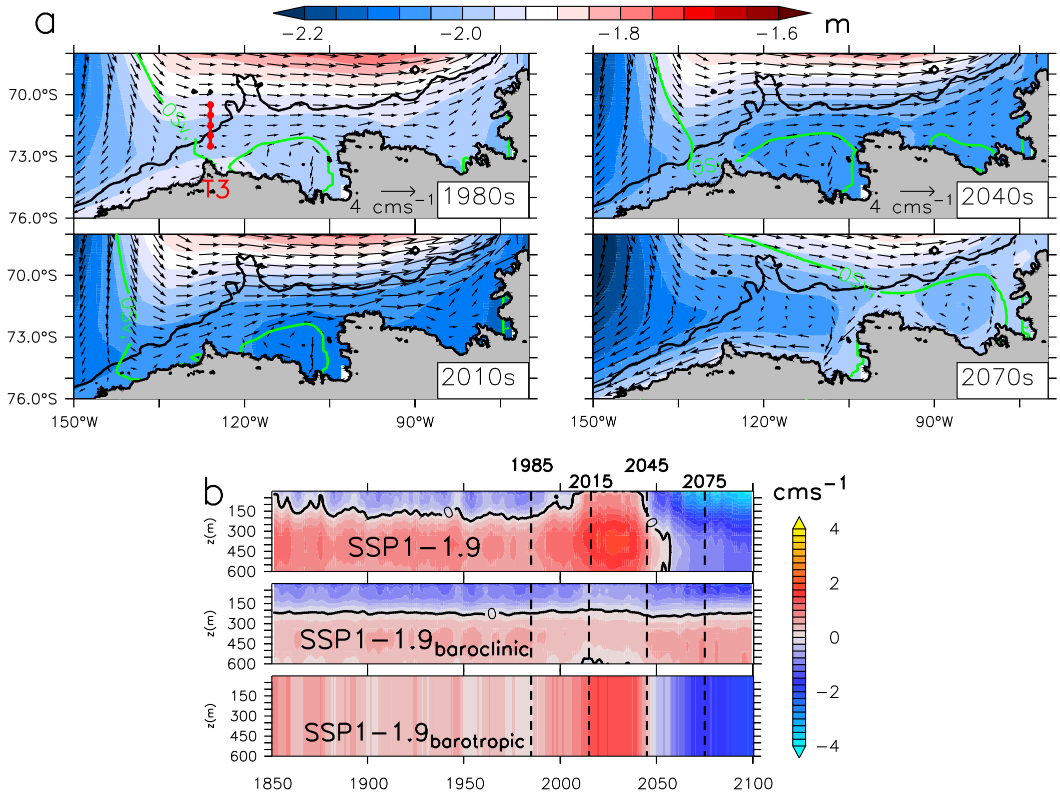

Figure 2. (a) Decadal averages of historical and SSP1-1.9 modelled ensemble-mean DOT [m] and barotrophic flow [cms^{-1}] during the 1980s, 2010s, 2040s, and 2070s; the transect T3, at 125°W, is shown in the upper left panel. (b) Hovmöller diagram of the ensemble-mean meridionally-averaged zonal velocity at transect T3 from historical and SSP1-1.9 simulations; the barotropic and baroclinic components are shown. For reference, the vertical dashed lines indicate the middle year of the decades 1980s, 2010s, 2040s, and 2070s relevant to the fields shown in the panels a. The historical-SSP5-8.5 ensemble-means exhibit similar results, with a more energetic RG intrusion into the Amundsen-Bellingshausen seas (Fig. S2).

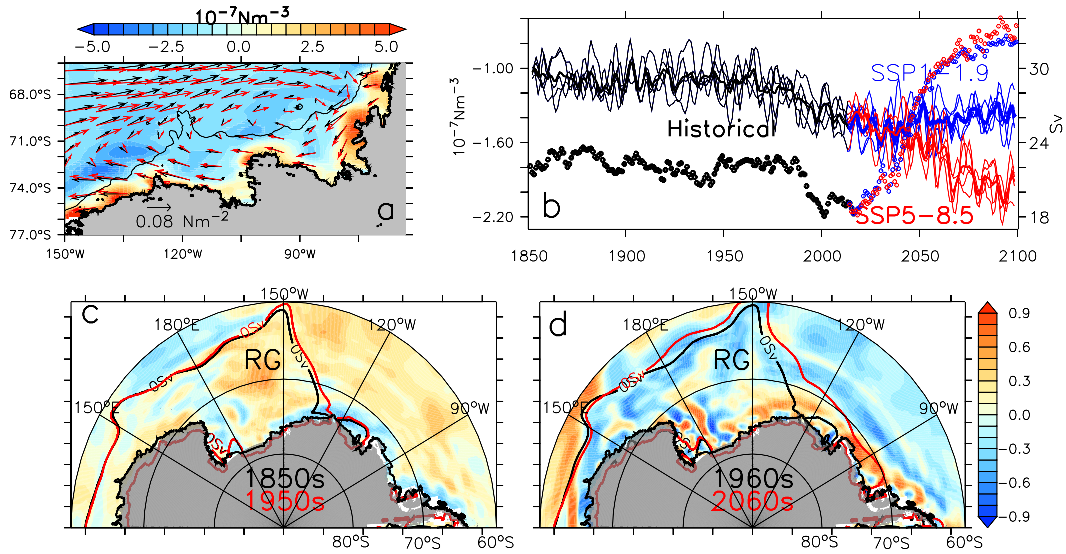

Figure 3. (a) Historical 1850-2014 average of ensemble-mean Ocean Surface Stress Curl (OSC) in color, overlain by decadal averaged ocean ensemble-mean surface stress vectors during the 1960s (black) and the 2040s (red). (b) Lines show spatial averages of OSC within the region shown in panel a, from the historical (black), SSP1-1.9 (blue), and SSP5-8.5 (red) experiments: thin lines are ensemble members and thick lines ensemble means. Circles show ensemble-mean Ross Gyre strength in Sverdrups (Sv). Maps of correlation between the ensemble-mean OSC and RG strength in SSP1-1.9 during the 1851-1960 and 1961-2070 periods are shown in panels (c) and (d), respectively. The averaged BSF_0 during the first (black) and last (red) decades are shown for each period. The SSP5-8.5 scenario exhibits similar correlation maps (not shown).

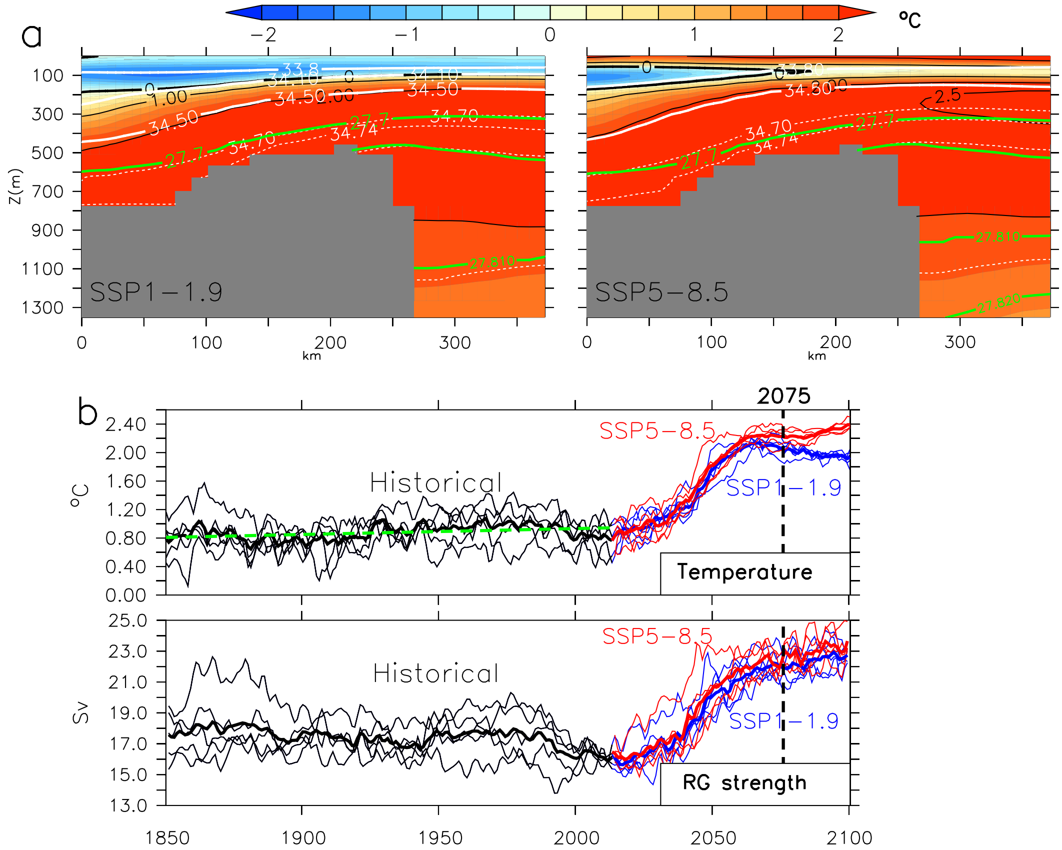

Figure 4. (a) 2070s averaged austral summer thermohaline structure along transect T1 from SSP1-1.9 and SSP5-8.5 ensemble means: both scenarios reproduce a warmer and saltier thermohaline structure than the one associated to the 1994-2018 historical period (Fig. 1e). White contours exhibit isohalines [psu], green countours correspond to the 27.7, 27.77, 27.81, and 27.82 potential density anomaly isopycnals [kg m^{-3}]. (b) Time series of the mean potential temperature on the Amundsen Sea shelf (within the 3000 m isobath, between 200 and 700 m depth, and between 115°W and 100°W) and mean RG strength. Thin and thick lines correspond to ensemble members and ensemble means, respectively. The green dashed line in the temperature panel is the modeled ∼0.12°C century^{-1} warming trend during the historical 1850-2014 period, similar to the warming trend reported by Naughten et al. (2022). For reference, the vertical dashed lines indicates the middle year of the 2070s decade, relevant to the averaged thermohaline fields shown in the upper panels.